RSC Advances

ROYAL SOCIETY OF CHEMISTRY

www.rsc.org/advances

Computational Study on the Mechanism and Kinetics for the Reaction between CH_3CH_2S and OH

Tianlei Zhang[a,*],　Rui Wang [a], Liting Zhou[a],　Zhiyin Wang[a],　Qiong Xu[a], Suotian Min[a],　　Wenliang Wang [b] *

[a] School of Chemical & Environment Science, Shaanxi University of Technology, Hanzhong, Shaanxi 723001, China

[b] Key Laboratory for Macromolecular Science of Shaanxi Province, School of Chemistry & Chemical Engineering, Shaanxi Normal University, Xi'an, Shaanxi 710062, China

Abstract The reaction mechanism of CH_3CH_2S with OH radical is studied at the CBS-QB3 level of theory. Five substitution process and eleven addition-elimination channels are identified for the title reaction. The calculated results indicate that addition-elimination channels CH_3CHS+H_2O, CH_2CH_2+HSOH, CH_3CHSO+H_2 and CH_3CH_2SH+O are dominant.

Other channels may be negligible due to the high barrier heights. Rate constants and branching ratios are estimated by means of the conventional transition state theory with zero curvature tunnelling over the temperature range of 200–3000 K. The calculation shows that the overall rate constant in the temperature of 200-3000 K is main dependent on the channels CH_3CHS+H_2O, CH_2CH_2+HSOH and CH_3CH_2SH+O. The three-parameter expression for the total rate constant is fitted to be $k_{\text{total}} = 7.42 \times 10^{-21} T^{2.63} \exp(-772.43/T)$ $cm^3 \cdot molecule^{-1} \cdot s^{-1}$ between 200-3000 K.

Keywords　$CH_3CH_2S\cdot$　OH ·　Mechanism · · Rate constant

* Corresponding authors. Tel: +86-0916-2641083, Fax: +86-0916-2641083.

e-mail: ztianlei88@163.com (T. L Zhang);　wlwang@snnu.edu.cn (W. L. Wang).

1. Introduction

CH$_3$CH$_2$S, CH$_3$S, CH$_2$SH, CH$_2$S and HCS and other sulfur-contained small organic molecules released from fuel combustion and oxidation of sulfur, has become one of the major pollution sources of atmospheric environment[1-3]. These sulfur-containing compounds have been widely studied because of their negative effects on the Earth's environment[4-8]. CH$_3$CH$_2$S is a typical representative of sulfur-contained small organic molecules, which is main product of laser photolysis of C$_2$H$_5$SSC$_2$H$_5$ or C$_2$H$_5$SH and also an important reaction intermediates[9-11]. Although this sulfur-contained small molecules shows a very low level in Earth's atmosphere, but it have a significant impact on climate change and acid rain formation. Therefore, the stability of this sulfur-contained small molecule, its reactivity with atmospheric free radicals and how to eliminate its effect on air pollution has attracted wide attention. OH are one of the most important atmospheric oxidant[12, 13]. Outer shells of OH have unpaired electron, it always tends to get electronics, with high activity, and thus the role of atmospheric trace constituents from strong oxidants, for many important compounds, reaction with OH is their degradation rate-determining step[14-16].

The reaction of sulfur-contained small molecules with OH radical is one of the most important degradation processes in the atmosphere[17-19]. Zhang et al [20] investigated the mechanism of the reaction of C$_2$H$_5$S with HO$_2$ at the CCSD(T)/aug-cc-pVDZ//B3LYP/6-311G(2d,p) method. They obtained both hydrogen abstraction and addition-elimination reaction pathways on the singlet and triplet potential surfaces. Cao et al [21]theoretically investigated the reaction mechanism of CH$_3$SCH$_2$CH$_3$ with OH at the CCSD(T)/6-311++G(d,p)//MP2/6-31+G(2d,p). They measured The CVT/SCT rate constants of hydrogen abstraction channels over the temperature range of 200-900 K. However, the reaction of CH$_3$CH$_2$S with OH has not been reported so far to the best of our knowledge.

The objective of the present study on the reaction of C$_2$H$_5$S with OH is to exploit its possible reaction pathways, to shed light on the reaction mechanism, to provide new insight into the new sink of aliphatic thiols in the atmosphere, and fundamental foundations for preventing and eliminating air pollutions from aliphatic thiols. So in this paper, the reaction mechanism of CH$_3$CH$_2$S with OH radical is studied. Then based on the obtained mechanism information, the rate constants of the major channel are calculated.

2. Computational method

The quantum chemistry calculations reported in this work were carried out with Gaussian 09[22] program packages. We used the B3LYP/CBSB7 and UB3LYP/CBSB7[23, 24] method to optimize and characterize the closed-shell and open-shell stationary points respectively. At this level of theory, we also calculated the harmonic vibrational frequencies to verify the nature of the corresponding stationary points (minima or transition state), to provide the zero-point vibrational energy (ZPE) and to determine the thermodynamic

2

contributions to the enthalpy and free energy. Moreover, to ensure that the transition states were connected to the desired reactants and products, we performed intrinsic reaction coordinate (IRC) [25-28]calculations. In order to obtain more accurate relative energies, based on the optimized geometries, we performed single-point CBS-QB3[29, 30] and CCSD(T)/aug-cc-pVTZ[31] for closed-shell and performed single-point UCBS-QB3 and UCCSD(T)/aug-cc-pVTZ calculations for open-shell stationary points. Finally, the kinetic properties of the system were calculated using conventional transition state theory (TST) [32-34] in the VKLab[35-37] program coupled with the steady state approximation.

These calculations made use of the energies obtained at the CBS-QB3 level of theory and the partition functions computed at the B3LYP/CBSB7 level of theory. The tunnelling correction to the rate constants was computed using the zero-order approximation of a vibrationally adiabatic potential energy surface (PES) with zero curvature. In this case, the unsymmetrical Eckart potential energy barrier was used to approximate the potential energy curve.

3. Results and discussion

The values $<S^2>$ of all the species involving the C_2H_5S+OH reaction were shown in Table S1. As illustrated in Table S1, after spin annihilation for the singlet, doublet and triplet species, the values of $<S^2>$ were respectively nearly 0.0000, 0.7500, and 2.0000 at the B3LYP/CBSB7 level of theory, so the spin contamination is not severe. All optimized geometries of the reactants, complexes, transition states, and products involving the nucleophilic substitution reaction and addition-elimination channels at the B3LYP/CBSB7 level of theory along with the available experimental[38-42] values were displayed in Figure 1, Figure 3, and Figure 5. For the species (OH, $^1CH_3CHS$, H_2O, $^1CH_2CH_2S$, $^1CH_2S$, CH_3, CH_3OH, CH_4, CH_2CH_2 and H_2), the mean absolute deviations of bond lengths and bond angles between the calculated values at the B3LYP/CBSB7 level of theory and the corresponding experiment ones are 0.006 Å and 0.06°, respectively. So the calculated bond lengths and angles at the B3LYP/CBSB7 level of theory are acceptable. Besides, experimental data is not available with which to judge the accuracy of our results, therefore Table S2 lists the relative energies (ΔE), enthalpies (ΔH(298)), and free energies (ΔG(298)) to the reactants (C_2H_5S+OH) at the CBS-QB3 level as well as the heats of formation for every channel evaluated by CCSD(T)/aug-cc-pVTZ//B3LYP/CBSB7 calculations. By comparing the reaction enthalpy results obtained with CCSD(T)/aug-cc-pVTZ//B3LYP/CBSB7 and CBS-QB3, energetic results agree to 1-2 kcal•mol^{-1}. Therefore, the CBS-QB3 level of theory was able to describe the title reaction reliably. So potential energy profile of nucleophilic substitution reaction and addition-elimination channels for the reaction of CH_3CH_2S with OH at the CBS-QB3 level of theory were presented in Figure 2, Figure 4, and Figure 6.

3.1 Reaction mechanism

Five substitution processes (R1-R5) and eleven addition-elimination channels (R6-R16) were modeled for the title reaction, which were listed in SchemeS1-S3, as well as Figures 2, 4, and 6, where "IM" and "IMF" denote post-reactant complex and pre-product complex of the corresponding reaction pathway, respectively. For simplicity, the singlet and triplet species are signed 1 and 3 as superscription.

3.1.1 Nucleophilic substitution mechanism

For the nucleophilic substitution reaction of C_2H_5S+OH, two singlet channels (Channels R1 and R2) and three triplet channels (Channels R3, R4 and R5) were modeled as depicted in Scheme S1 and Figure 2.

Singlet channels of Channel R1 and R2 proceeded by the oxygen atom of OH radical respectively attacking to the carbon atom of α–CH_2 and β-CH_3, simultaneously C(1)-C(2) bond breaking. The corresponding transition state was TS1 and TS2, respectively. In TS1, the breaking C(1)-C(2) bond shown in Figure 1 was elongated by 0.686 Å compared with that in CH_3CH_2S, while the forming O-C(2) bond was 0.630 Å longer than that in SCH_2OH. In TS2, the breaking C(1)-C(2) bond is elongated by 0.359 Å compared with that in CH_3CH_2S, while the forming O-C(2) bond is 0.495 Å longer than that in CH_3OH. The barrier height of Channel R1 and R2 was 24.78 and 18.23 kcal·mol^{-1}, respectively.

Similar with singlet Channel R1, the triplet oxygen-to-(α)carbon nucleophilic substitution channel (R3) is also located to produce $SCH_2OH + CH_3$. The barrier height of Channel R3 is 31.95 kcal·mol^{-1}, which is higher by 7.17 kcal·mol^{-1} than that of the singlet channel R1, showing that the formation of $SCH_2OH + CH_3$ mainly take from Channel R1. The triplet oxygen-to-(β) carbon nucleophilic substitution channel (R4) is located to produce $CH_3OH + {}^3CH_2S$ with the energy barrier of 33.34 kcal·mol^{-1}. Compared with the barrier of singlet oxygen-to-(β) carbon nucleophilic substitution channel (R2), the barrier height of Channel R4 is higher by 15.11 kcal·mol^{-1}, indicating that oxygen-to-(β) carbon nucleophilic substitution reaction mainly occurs on the singlet potential energy surface.

Differently from singlet nucleophilic substitution reaction that oxygen-to-sulfur nucleophilic substitution could not taken place due to the stability of ${}^1CH_3CH_2SOH$, the triplet oxygen-to-sulfur nucleophilic substitution channel (R5) is located to produce $CH_3 + CH_2SOH$. The barrier height of Channel R5 was 30.02 kcal·mol^{-1}. This was lower by 1.93-3.32 kcal·mol^{-1} than that of triplet Channels R3 and R4, but it was higher by 5.24-11.29 kcal·mol^{-1} than that of singlet Channels R1 and R2. From above mechanism elucidation, it can be concluded that triplet nucleophilic substitution mechanisms are more unfeasible than the singlet because of the higher barrier heights. The nucleophilic substitution reaction of C_2H_5S+OH should mainly occur on the singlet PES. Moreover, singlet oxygen-to-(β) carbon nucleophilic substitution channel (R2) is most favorable nucleophilic substitution channel.

4

3.1.2 Addition-elimination mechanism

For the addition-elimination reaction of C_2H_5S+OH, four channels (Channels R6- R9) of H_2O formation were modeled as depicted in Scheme S2 and Figure 4, meanwhile seven channels (Channels R10- R16) of CH_4, C_2H_4, H_2, CH_3CH_2SH and CH_3OH formations were modeled as depicted in Scheme S3 and Figure 6.

3.1.2.1 The channel of H_2O formation

Five hydrogen atoms of the CH_3CH_2S are distributed into the two groups, which are, H atom in α-CH_2(α-position carbon atom adjacent to the sulfur atom) and β-CH_3 (carbon atom stands away from the sulfur atom). Thus, two possible reaction of hydrogen abstraction from CH_3CH_2S by OH radical are investigated on both singlet and triplet potential energy surface (singlet channels (R6 and R7) and triplet channels (R8 and R9)). Moreover, similar with the reaction between $CH_3SCH_2CH_3$ and OH[43], each reaction can occur in more than one pathway due to the effect of sulfur atom of CH_3CH_2S.

Before the transition state and the products, singlet channels R6 and R7 (shown in Figure 4) begin with the $^1CH_3CH_2SOH$ intermediate, whose structure is loose with the O atom of OH and the S atom of CH_3CH_2S separation of 1.699 Å. The relative energy of $^1CH_3CH_2SOH$ to the reactants (CH_3CH_2S +OH) is -69.82 kcal·mol^{-1} at the CBS-QB3 level of theory. For channel R6, starting from $^1CH_3CH_2SOH$, products (CH_3CHS+H_2O) were obtained via transition state TS6a, TS6b, which were labeled as Path R6a and R6b, respectively. Transition state TS6a, and TS6b differentiated mainly from each other in the relative orientation of the hydrogen atoms of OH radical. Such geometrical discrepancy may leads that TS6b was only lower by 0.12 kcal·mol^{-1} than that of TS6a.

For channel R7, beginning with $^1CH_3CH_2SOH$, products ($CH_2CH_2S+H_2O$) can be obtained via TS7a and TS7b, respectively. The difference between TS7a and TS7b mainly lies in dihedral angle $\angle H(10)OH(4)C(1)$ (in Figure 3). Hydrogen atom of the OH radical is directed toward the sulfur atom in TS7a ($\angle H(10)OH(4)C(1)=109.8°$), while it is stays away from the sulfur atom in TS7b ($\angle H(10)OH(4)C(1)=-92.6°$). The imaginary frequencies of TS7a and TS7b are 1490i cm^{-1} and 1602i cm^{-1}, respectively. The relative energy of TS7a and TS7b to the reactants (CH_3CH_2S +OH) is respectively -2.04 and -2.40 kcal·mol^{-1}, which is higher by 15.60-15.84 kcal·mol^{-1} than that of TS6a (-17.88 kcal·mol^{-1}) and TS6b (-18.00 kcal·mol^{-1}), indicating that, for singlet H-abstraction channels, Channel R6 is easily to occur for the lower barrier heights compared to channel R7.

Similar to the singlet H-abstraction processes (Channels R6 and R7), the corresponding triplet α-CH_2 site and β-CH_3 site H-abstraction reaction were found beginning with the formation of intermediate $^3CH_3CH_2SOH$ before the transition state and the products. From the geometrical point of view as depicted in Figure 3, the bond distance between the O atom of OH and the S atom of CH_3CH_2S in $^3CH_3CH_2SOH$ complex is stretched by 0.419 Å compared

with the corresponding bond distance in $^1CH_3CH_2SOH$. Such discrepancy may lead that the relative energy of $^3CH_3CH_2SOH$ to the reactants (CH_3CH_2S +OH) is higher by 59.5 kcal·mol$^-$ ^{1} than that of $^1CH_3CH_2SOH$ to the reactants (CH_3CH_2S +OH). Starting from $^3CH_3CH_2SOH$ complex, triplet α-CH_2 site and β-CH_3 site H-abstraction reaction occurs *via* Channel R8 (TS8a, TS8b) and Channel R9 (TS9a, TS9b and TS9c), respectively. Compared with the corresponding transition states in singlet H-abstraction processes (Channels R6 and R7), triplet transition states shown in Figure 3 were different in two respects. First, there is not the formation of S-O bond in triplet transition states. Second, the C-H-O bond angle in triplet transition state is less bent (e.g., ∠O(4)H(5)C(1) 134.7° in TS6a *vs* 160.3° in TS8a; ∠O(4)H(7)C(2) 154.4° in TS7a *vs* 173.4° in TS9a). It is shown in Figure 4 that the relative energy of TS8a and TS8b in Channel R8 is lower by 1.23-5.91 kcal·mol^{-1} than that of the TS9a, TS9b and TS9c in Channel R9. This indicates that triplet α-CH_2 H-abstraction reaction (Channel R8) is easily to take place than triplet β-CH_3 site H-abstraction reaction (Channel R9). However, compared with singlet α-CH_2 H-abstraction reaction (Channel R6), the relative energy of TS8a and TS8b in Channel R8 is higher by 16.70-17.34 kcal·mol^{-1} than that of the TS6a, and TS6b in Channel R1.

According to the discussed above, for the activity of hydrogen abstraction, the singlet channels are stronger than triplet channel, and for the activity of hydrogen abstraction of the singlet channel, the α-carbon atom is stronger than *β*-carbon atom (the order is: α-CH_2 (R6)＞ β-CH_3 (R7)＞α-CH_3 (R8)>β-CH_3 (R9). Atomic Mulliken charge of α-carbon atom (*α*-CH_3, 0.0464e) is more electropositive than that of β-CH_3 (0.1231e), which leads to the C-H bond of α-position weaker than that of *β*-position. On the other hand, the stability orders of the product radicals, $^1CH_3CHS$＞$^1CH_2CH_2S$＞$^3CH_3CHS$> $^3CH_2CH_2S$, produced by R6, R7, R8 and R9, respectively, is in consistent with the activity order of hydrogen abstraction. This is possibly because the substituent at the unpaired electron position influences on the stability of the above-mentioned radicals.

3.1.2.2 The channels of CH$_4$ formation

As described above that $^1CH_3CH_2SOH$ was much more stable than $^3CH_3CH_2SOH$, all the addition-elimination channels R10-R16 were taken into account beginning with pre-reactant complex $^1CH_3CH_2SOH$. Similar with the reaction between CH_3 and C_2H_5OH[44], Channels R10 and R11 in Figure 6 have been considered that the C atom of CH_3 respectively abstracts the hydrogen atom from C(1) and O(4) sites in $^1CH_3CH_2SOH$ with the H_3C•••H-X bond (where X denotes HCSOH and CH_2SO) in their transition states. For Channel R10, as shown in Figure 5, one of the two H atoms of the CH_2 group in $^1CH_3CH_2SOH$ can migrate toward the C atom in the CH_3 group to produce CH_4 +HCSOH via TS10. The breaking C(1)-C(2) bond was elongated from 1.523 Å in $^1CH_3CH_2SOH$ to 2.198 Å in TS10. The barrier height of R10 was 79.09 kcal·mol^{-1}. Channel R11 leads to the formation of CH_4+CH_2SO via TS11. The product

6

CH$_2$SO can be further formed to cyclic geometry (c-CH$_2$SO) via transition state TS11-1 with the barrier height of 52.11 kcal·mol^{-1}. The breaking O-H bond in TS11 was 1.216 Å much longer than the corresponding value in ^{1}CH$_3$CH$_2$SOH. The forward potential barrier of Channel R11 at the CBS-QB3 level was 74.52 kcal·mol^{-1}, which was lower by 4.57 kcal·mol^{-1} than that of Channel R10. The higher C-H dissociation energy (C-H, 473.0 kJ·mol^{-1}; O-H, 436.0 kJ·mol^{-1}) of CH$_2$SOH moiety may be responsible for the higher barrier of Channel 10.

3.1.2.3 The channels of C$_2$H$_4$ formation

For Channel R12, our result presented in Figure 5 shows that HOSH elimination from ^{1}CH$_3$CH$_2$SOH occurs via a four-centered (H(9)-S(3)-C(2)-C(1)) transition state TS12 with C_1 symmetry. The dihedral angle of the H atom in the four centered-ring H(9)-S(3)-C(2)-C(1) is -0.5°. The breaking C-H and C-S bonds in TS12 are 0.333 and 0.552 Å longer than those in ^{1}CH$_3$CH$_2$SOH. TS12 lies below the reactants C$_2$H$_5$S+OH by 13.28 kcal·mol^{-1} at the CBS-QB3 level, which is respectively lower by 22.55 kcal·mol^{-1} and 17.98 kcal·mol^{-1} than the corresponding values of TS10 and TS11. This indicates that HOSH elimination (Channel R12) is much favorable than the C atom of CH$_3$ respectively abstracts the hydrogen atom from C(1) and O(4) sites in ^{1}CH$_3$CH$_2$SOH (Channels R10 and R11) kinetically.

3.1.2.4 The channels of H$_2$ formation

As shown in Figure 5, Channels R13 and R14 are the C-H cleavage and the H$_2$-elimination reactions. Differently from Channel R13 that the H atom of the OH group and one of the two H atoms from the CH$_2$ group in ^{1}CH$_3$CH$_2$SOH form H$_2$ via HHO(4)S(3)C(1) five-member-ring transition state TS13, in Channel R14, two H atoms each from the CH$_3$ and OH groups in ^{1}CH$_3$CH$_2$SOH, form a HHO(4)S(3)C(1)C(2) six-member-ring transition state TS14, resulting in H$_2$ elimination to produce H$_2$, CH$_2$=CH$_2$ and SO. Comparing the two H$_2$-elimination processes in Channels R13 and R14, we see that TS14 is about 11.58 kcal·mol^{-1} higher than TS13. The difference may be ascribed to the fact that a strong stereo repulsion force from the CH$_3$ group exists and additional C(1)-S(3) bond breaking in TS14.

3.1.2.5 The channels of CH$_3$CH$_2$SH and CH$_3$OH formation

As shown in Figure 5, we also calculated other reaction channels consisting CH$_3$CH$_2$SH+O (Channel R15) and CH$_3$OH+ CH$_2$S (Channel R16) channels. Channel R16 may be negligible for the high relative energy (9.45-34.13 kcal·mol^{-1}) of TS16 to the transition states TS10-TS15. Such energy discrepancy is possibly due to the two bonds (S(3)-O(4) and C(1)-C(2)) cleavage, which makes the Channel R16 much harder. For Channel 15, starting from ^{1}CH$_3$CH$_2$SOH complex, the isomerization process (^{1}CH$_3$CH$_2$SOH→ TS15→CH$_3$CH$_2$SHO) takes place by the S atom abstracts hydrogen atom from OH site in ^{1}CH$_3$CH$_2$SOH. This reaction channel includes the O(4)-H(10) dissociation and S(3)-H(O(4))

7

bond formation. The O(4)-H(10), and S(3)-H(O(4)) bond lengths in TS15 is 1.479 and 1.394 Å, respectively. The transition states TS15 show three-member-ring structures (H(10)-O(4)-S(3)) and has a barrier of 58.02 kcal·mol^{-1}, which is only higher by 1.48 kcal·mol^{-1} than that of Channel 12. This indicates that Channel R15 also occurs easily.

In summary, addition-elimination channels R6, R12, R13 and R15 are the major channels. Other channels may be negligible due to the high barrier heights. Furthermore, the lowest barrier for the channel CH$_3$CHS +H$_2$O is $\sim$ 5 kcal·mol^{-1} lower than that of the addition-elimination channel CH$_2$CH$_2$ +HSOH, which is similar with the reactions of ethanol[45] (the lowest energy channel is the H$_2$O-formation reaction).

3.3 Rate constant calculation for major channels
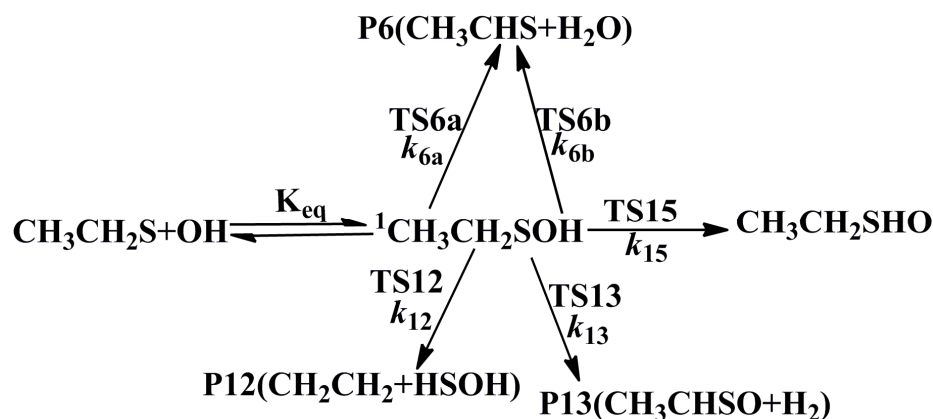
Scheme 1 The selected reaction channels in rate constant calculations

The rate constant calculations of the selected channels were shown in Scheme 1, where "TS" and "K$_{eq}$" denote the transition state and equilibrium constant of the corresponding reaction pathway, respectively. k denotes the rate constant of the corresponding reaction pathway. We neglect the rate constant calculation of channel R1-R5, R7-R11, R14 and R16 because of their high barriers. Reaction channels R6, R12, R13 and R16 all began with the formation of a prereactive complex before progressing through the transition state, which is depicted in equation (1).

$$C_2H_5S+OH \underset{k_{-1}}{\overset{k_1}{\longleftrightarrow}} {}^1C_2H_5SOH \xrightarrow{k_2} products \qquad (1)$$

Assuming that the prereactive complex $^1C_2H_5SOH$ was in equilibrium with the reactants and was at steady state, the overall rate constant was expressed as

$$k = \frac{k_1}{k_{-1}+k_2}k_2 \qquad (2)$$

If $k_2 \ll k_{-1}$, the rate constant was rewritten as

$$k = \frac{k_1}{k_{-1}+k_2}k_2 = K_{eq}k_2 \qquad (3)$$

where K_{eq} and k_2 were given by equation (4) and the VKLab program[35], respectively.

$$K_{eq}(T) = \sigma \frac{Q_{CR}}{Q_{R1}Q_{R2}} \exp(\frac{E_R - E_{CR}}{RT}) \qquad (4)$$

The various Q values denoted the partition functions of the intermediates, reactants C_2H_5S and OH. E_R, E_{CR} are the total energies of the reactants and the post-reactant complex CR; σ is the symmetry number.

In the rate constant calculation, the overall rate constant k_{total} are calculated within the temperature range of 200-3000 K, which was given by $k_{total} = K_{eq} \times (k_{6a} + k_{6b} + k_{12} + k_{13} + k_{15})$. Figure 7 and Table S3 lists the temperature dependence of $k_{R6}(k_{R1}=K_{eq}\times(k_{6a}+k_{6b}))$, $k_{R12}(k_{R12}=K_{eq}\times k_{12})$, $k_{13}(k_{13}=K_{eq}\times k_{13})$, k_{15} $(k_{R15}=K_{eq}\times k_{15})$ and k_{total} within the temperature range of 200-3000 K. In the calculated temperature range, k_{R6}, k_{R12}, k_{13}, k_{15} and k_{total} all decrease slowly at low temperature, and increase at high temperature range. Such as, as the temperature increases, k_{total} decreases slowly in the temperature range of 200-298 K ($k_{total}^{298}/k_{total}^{200} = 0.88$), and increases within the temperature range of 298-3000 K ($k_{total}^{3000}/k_{total}^{295} = 13.1$). The branching ratios of channel R6, R12, R13 and R15 are described in Figure 8 and Table S4. It can be seen in Figure 8 and Table S4 that the overall rate constant in the temperature of 200-3000 K is main dependent on the R6, R12 and R15. At 200 K, the contribution of R1($k_6 k_{total}$), R12(k_{15}/k_{total}) and R15((k_{15}/k_{total})) to the total rate constant is 50.0%, 25.0%, 18.0%, respectively.. As the temperature increases, R6 and R12 become significant (k_6/k_{total}, 66.0%, k_{12}/k_{total}, 28.0 %, k_{15}/k_{total}, 5.0 % at 3000 K). The contribution of R13 to the overall rate constant over the temperature of 200-3000 K is small within 7%.

For kinetic modeling applications, the calculated TST rate constant k_6, k_{12}, k_{13}, k_{15} and k_{total} in the temperature range of 200-3000 K have been fitted to the three-parameter expressions (unit in cm^3·molecule^{-1}·s^{-1}):

$$k_6 = 2.77 \times 10^{-21} T^{2.71} \exp(-751.02/T)$$

$$k_{12} = 3.00 \times 10^{-21} T^{2.60} \exp(-714.11/T)$$

$$k_{13} = 7.13 \times 10^{-22} T^{2.35} \exp(-1054.81/T)$$

$$k_{15} = 4.97 \times 10^{-20} T^{2.02} \exp(-711.46/T)$$

$$k_{total} = 7.42 \times 10^{-21} T^{2.63} \exp(-772.43/T)$$

4. Conclusions

Theoretical method CBS-QB3 is applied to study the reaction mechanism of CH_3CH_2S with OH. The rate constants of major channels are evaluated over the temperature range of 200-3000 K. The main conclusions are summarized as follows:

(1) Two mechanisms are investigated for the title reaction, namely, substitution and addition-elimination. Addition-elimination channels CH_3CHS+H_2O, CH_2CH_2+HSOH, $CH_3CHSO+H_2$ and CH_3CH_2SH+O are the major channels.

(2) The overall rate constant in the temperature of 200-3000 K is main dependent on the channels CH_3CHS+H_2O, CH_2CH_2+HSOH and CH_3CH_2SH+O. The contribution of channel $CH_3CHSO+H_2$ to the overall rate constant over the calculated temperature is small within 7%.

Acknowledgements

References

1 K. Torén, S. Hagberg and H. Westberg, *Am J Ind Med*, 1996, **29**, 111-122.
2 S. Aloisio, *Chemical Physics*, 2006, **326**, 335-343.
3 I. Barnes, J. Hjorth and N. Mihalopoulos, *Chem Rev*, 2006, **106**, 940-975.
4 N. González-García, À. González-Lafont and J. M. Lluch, *J. Comput. Chem.*, 2005, **26**, 569-583.
5 K. Wang, L. Du and M. Ge, *J Environ Sci*, 2009, **21**, 137-141.
6 A. M. El-Nahas, T. Uchimaru, M. Sugie, K. Tokuhashi and A. Sekiya, *Journal of Molecular Structure: THEOCHEM*, 2005, **722**, 9-19.
7 J. Jee and F.-M. Tao, *J. Phys. Chem. A*, 2006, **110**, 7682-7689.
8 B. P. Lomans, C. van der Drift, A. Pol and H. J. M. Op den Camp, *CMLS Cell Mol Life Sci* 2002, **59**, 575-588.
9 Z. X. Ma, C. L. Liao, H. M. Yin, C. Y. Ng, S.-W. Chiu, N. Ling Ma and W.-K. Li, *Chem. Phys. Lett.*, 1993, **213**, 250-256.
10 Y. S. Cheung, C. W. Hsu and C. Y. Ng, *J Electron Spectros Relat Phenomena*, 1998, **97**, 115-120.
11 C.-Y. Ng, *Annu Rev Phys Chem*, 2002, **53**, 101-140.
12 M. B. Williams, P. Campuzano-Jost, A. J. Hynes and A. J. Pounds, *J. Phys. Chem. A*, 2009, **113**, 6697-6709.
13 A. Cruz-Torres and A. Galano, *J. Phys. Chem. A*, 2007, **111**, 1523-1529.
14 A. Galano, *J. Phys. Chem. A,*, 2006, **110**, 9153-9160.
15 C. Zavala-Oseguera, J. R. Alvarez-Idaboy, G. Merino and A. Galano, *J. Phys. Chem. A,*, 2009, **113**, 13913-13920.
16 R. Crehuet, J. M. Anglada and J. M. Bofill, *Chem.-Eur. J. *, 2001, **7**, 2227-2235.
17 S. J. Baboukas. E, and N. Mihalopoulos, *Atmos Environ*, 2002, **36**, 5131-5139.
18 N. J. Zhu L, Wine PH, *J. Phys. Chem. A,*, 2005, **109**, 3903-3911.
19 R. M. Kirchner B, *J. Am. Chem. Soc.*, 2002, **124**, 6206-6215.
20 Y. Zhang, W. Zhang, T. Zhang, W. Tian and W. Wang, *Comput. Theor. Chem*, 2012, **994**, 65-72.
21 J. Cao, W. Wang, Y. Zhang, W. Wang, T. Zhang, J. Lv and C. Li, *Theor Chem Acc*, 2011, **129**, 771-780.
22 Frisch MJ, Trucks GW, Schlegel HB, Scuseria GE, Robb MA, Cheeseman JR, Scalmani G, Barone V, Mennucci B, Petersson GA et al (2004) Gaussian 09, revision A.01. Gaussian, Inc., Wallingford.
23 A. D. Becke, *J. Chem. Phys. *, 1993, **98**, 5648-5652.
24 C. Lee, W. Yang and R. G. Parr, *Phys. Rev. B*, 1988, **37**, 785-789.

25 K. Fukui, *Accounts of Chemical Research*, 1981, **14**, 363-368.
26 M. Page and J. W. McIver, 1988, **88**, 922-935.
27 C. Gonzalez and H. B. Schlegel, *J. Chem. Phys.*, 1989, **90**, 2154-2161.
28 C. Gonzalez and H. B. Schlegel, *J. Phys. Chem.*, 1990, **94**, 5523-5527.
29 J. A. Montgomery, M. J. Frisch, J. W. Ochterski and G. A. Petersson, *J. Chem. Phys.*, 1999, **110**, 2822-2827.
30 B. Sirjean, E. Dames, H. Wang and W. Tsang, *J. Phys. Chem. A*, 2012, **116**, 319-332.
31 J. A. Pople, M. Head‑Gordon and K. Raghavachari, *J. Chem. Phys.*, 1987, **87**, 5968-5975.
32 B. C. Garrett and D. G. Truhlar, *J. Chem. Phys.*, 1979, **70**, 1593-1598.
33 B. C. Garrett and D. G. Truhlar, *J. Am. Chem. Soc.*, 1979, **101**, 4534-4548.
34 B. C. Garrett, D. G. Truhlar, R. S. Grev and A. W. Magnuson, *J. Phys. Chem.*, 1980, **84**, 1730-1748.
35 Zhang, SW.; Truong, NT. VKLab version 1.0, University of Utah: Salt Lake City, 2001.
36 C.-M. Gong, Z.-R. Li and X.-Y. Li, *Energy Fuels*, 2012, **26**, 2811-2820.
37 W. T. Duncan, R. L. Bell and T. N. Truong, *J. Comput. Chem.*, 1998, **19**, 1039-1052.
38 A. R. Hoy and P. R. Bunker, *J. Mol. Spectrosc.*, 1979, **74**, 1-8.
39 K. Okiye, C. Hirose, D. G. Lister and J. Sheridan, *Chem Phys Lett*, 1974, **24**, 111-113.
40 D. J. Clouthier, G. Huang, A. G. Adam and A. J. Merer, *J. Chem. Phys.*, 1994, **101**, 7300-7310.
41 P. Venkateswarlu and W. Gordy, *J. Chem. Phys.* , 1955, **23**, 1200-1202.
42 E. Herbst, J. K. Messer, F. C. De Lucia and P. Helminger, *J Mol Spectrosc*, 1984, **108**, 42-57.
43 J. Cao, W. Wang, Y. Zhang, W. Wang, T. Zhang, J. Lv and C. Li, *Theor Chem Acc*, 2011, **129**, 771-780.
44 Z. F. Xu, J. Park and M. C. Lin, *J. Chem. Phys.*, 2004, **120**, 6593-6599.
45 J. Park, R. S. Zhu and M. C. Lin, *J. Chem. Phys.*, 2002, **117**, 3224-3231.

Figure Captions

Fig. 1 The geometrical structures of the optimized transition states products and imaginary frequencies (v, cm^{-1}) of transition states involving the singlet and triplet nucleophilic substitution reaction of C_2H_5S+OH at the CBS-QB3 level of theory.

Fig. 2 Schematic energy diagram for the singlet and triplet nucleophilic substitution reaction of C_2H_5S+OH at the CBS-QB3 level of theory

Fig. 3 The geometrical structures of the optimized reactants, transition states, intermediates, products and imaginary frequencies (v, cm^{-1}) of transition states involving the singlet and triplet channels of H_2O formation in the addition-elimination reaction of C_2H_5S+OH at the CBS-QB3 level of theory

Fig. 4 Schematic energy diagram for the singlet (a) and triplet (b) channels of H_2O formation in the addition-elimination reaction of C_2H_5S+OH at the CBS-QB3 level of theory

Fig. 5 The geometrical structures of the optimized transition states, intermediates, products and imaginary frequencies (v, cm^{-1}) of transition states involving the singlet addition-elimination reaction of C_2H_5S+OH at the CBS-QB3 level of theory

Fig. 6 Schematic energy diagram for the singlet addition-elimination reaction of C_2H_5S+OH at the CBS-QB3 level of theory

Fig. 7 Rate constants calculated in this work are plotted as a function of temperature (200–3000 K). k_{R6} ($k_{R6} = K_{eq} \times (k_{6a} + k_{6b})$) is rate constant for channel R6. k_{R12} is rate constant of channel R12, k_{R13}($k_{R13} = K_{eq} \times k_{13}$) is rate constant of channel R13, k_{R15} is rate constant of channel R15, k_{total} is the sum of k_{R6}, k_{R12}, k_{R13} and k_{R15}.

Fig. 8 The predicted branching ratios over the temperature range of 200–3000 K. The k_{R6}/k_{total}, k_{R12}/k_{total}, k_{R13}/k_{total} and k_{R15}/k_{total} represent the branching ratios of channel R6, R12, R13 and R15, respectively.

12

Fig. 1

Fig. 2

Fig. 3

15

Fig. 4

Fig. 5

Fig. 6

18
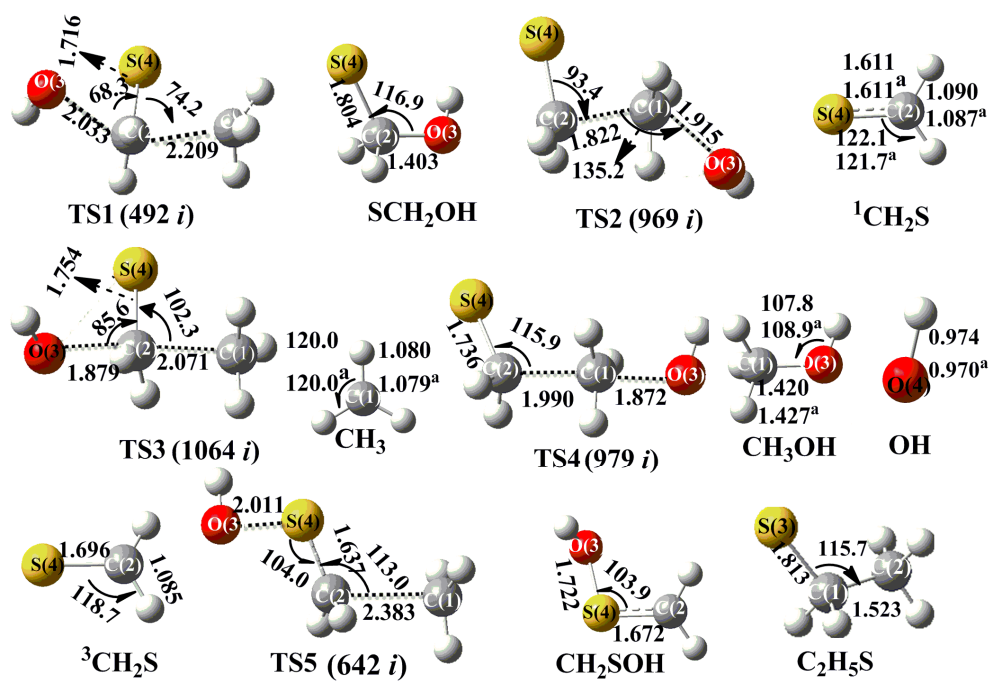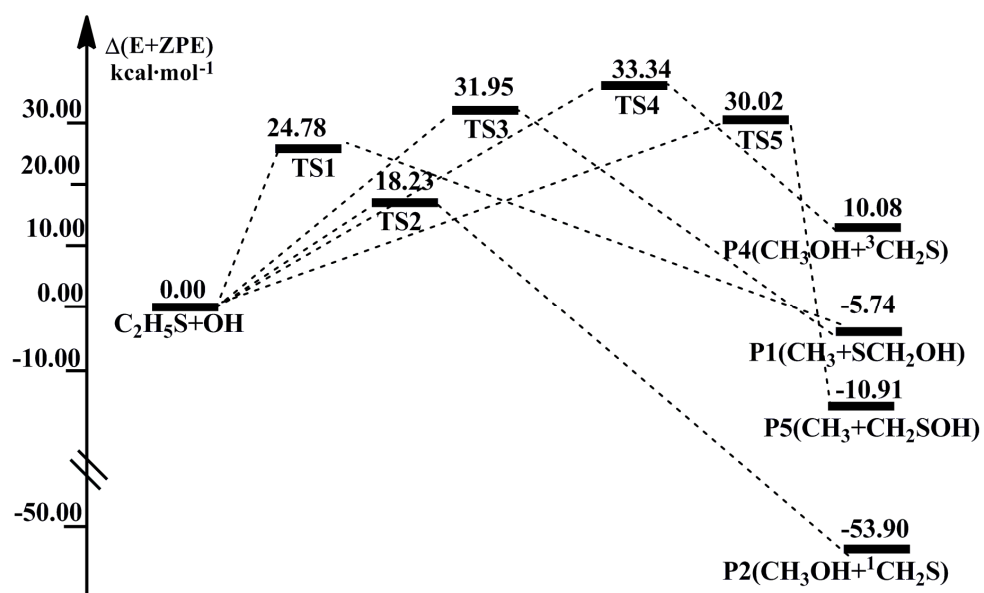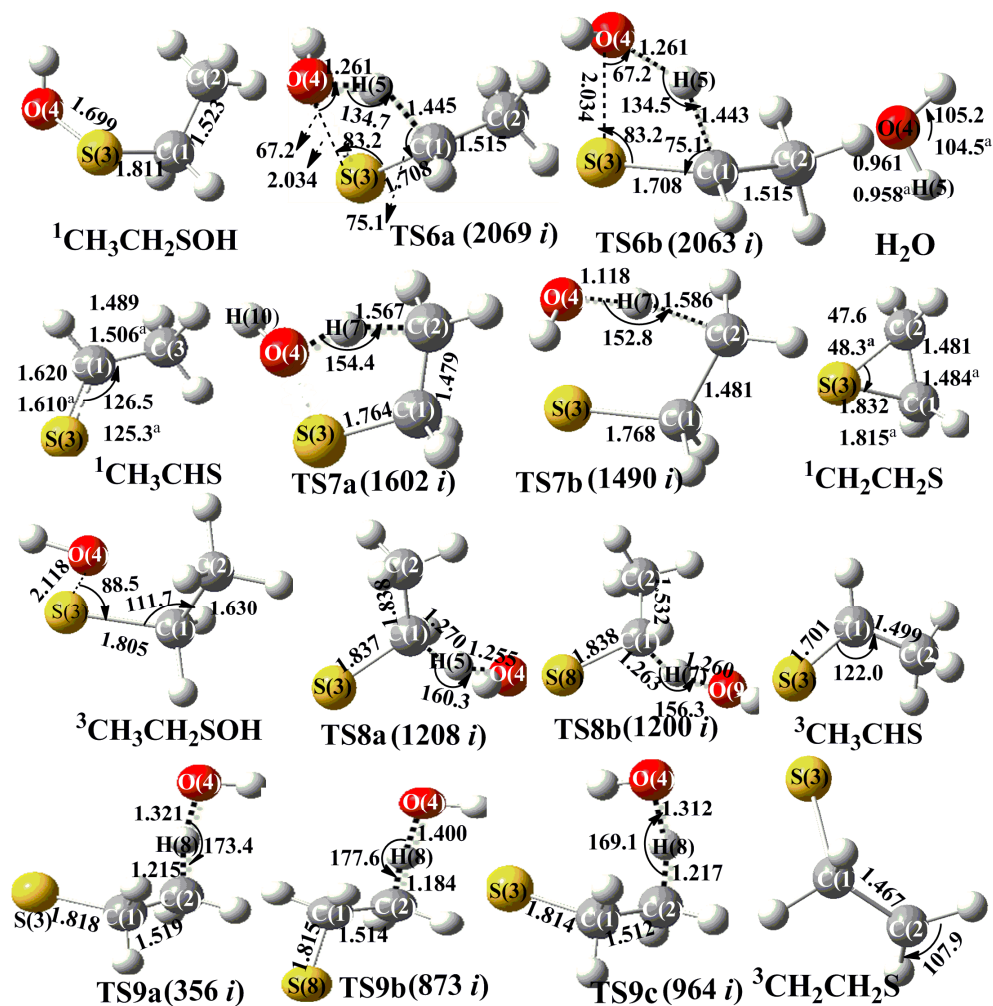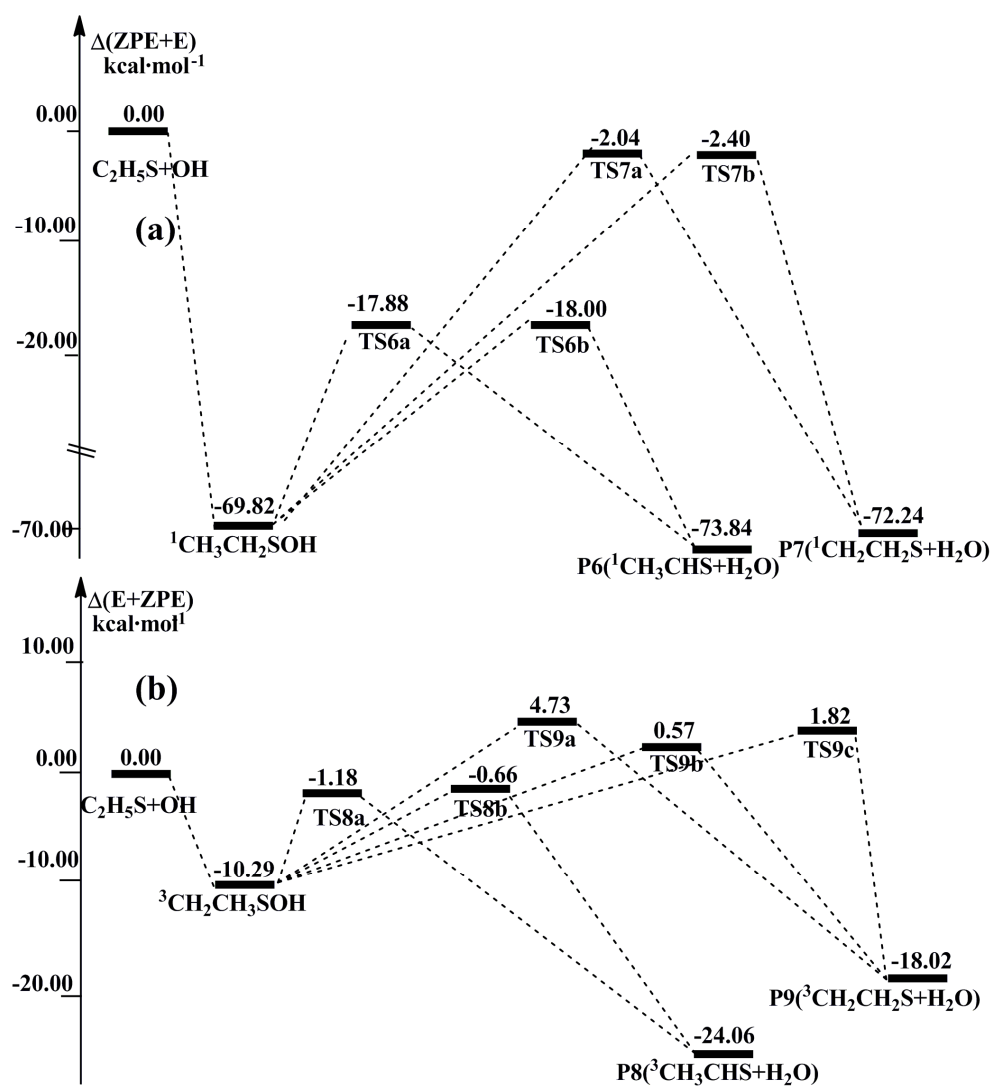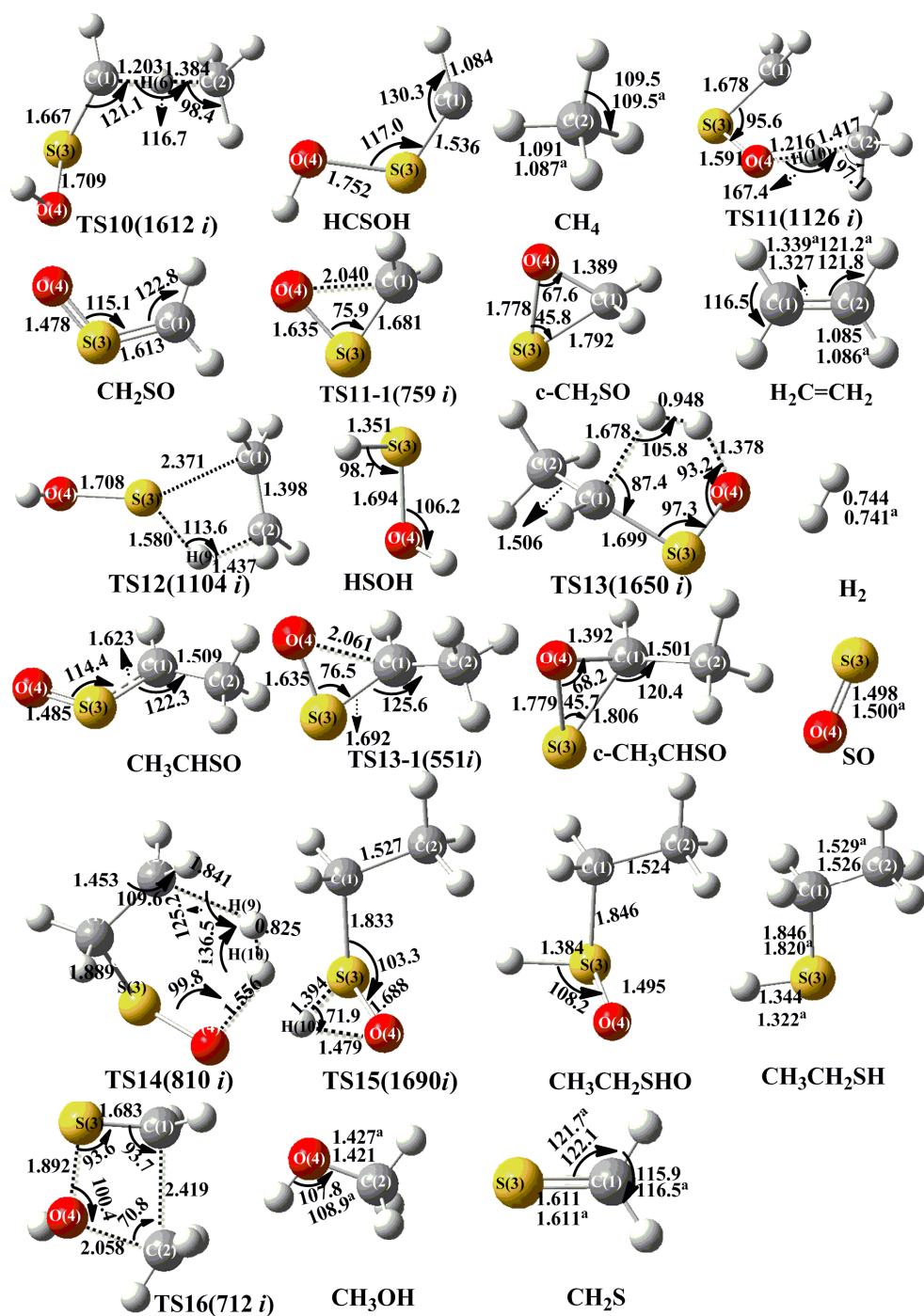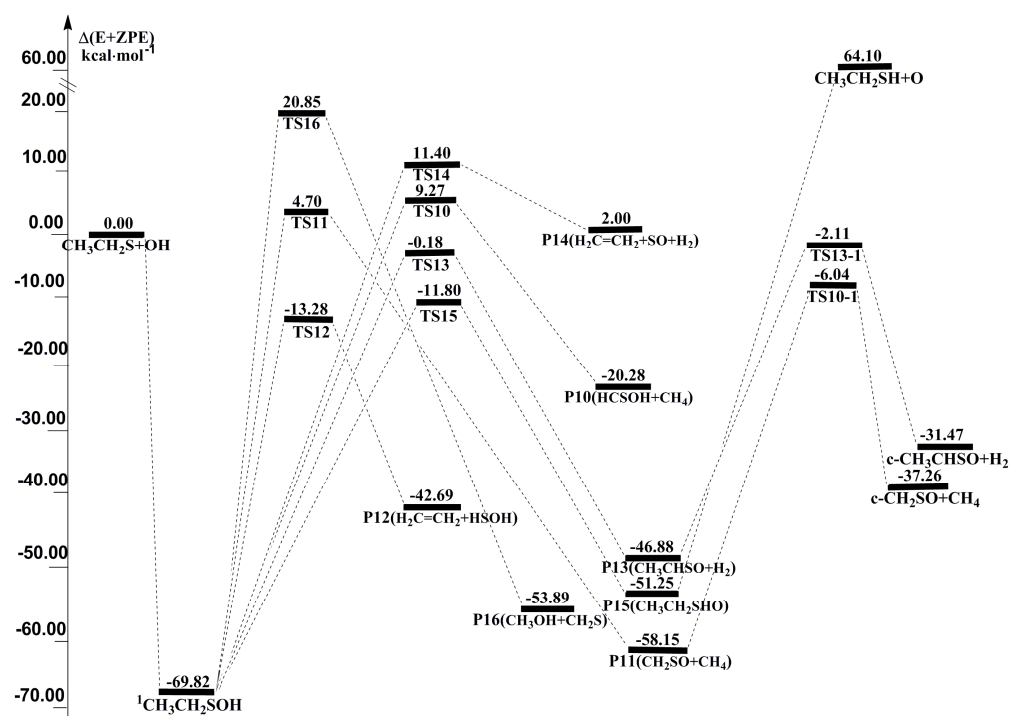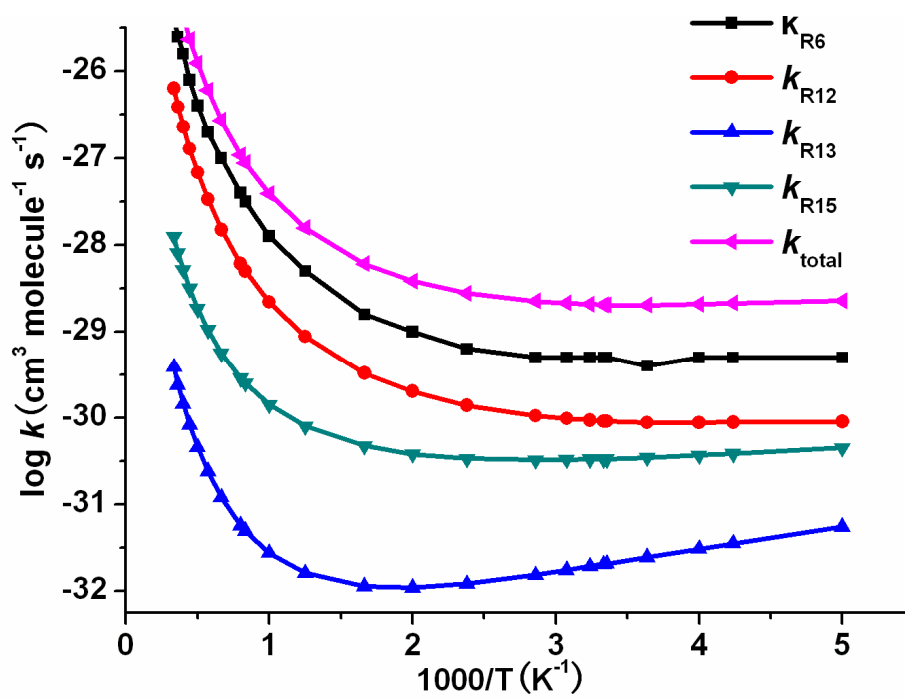
Fig. 7
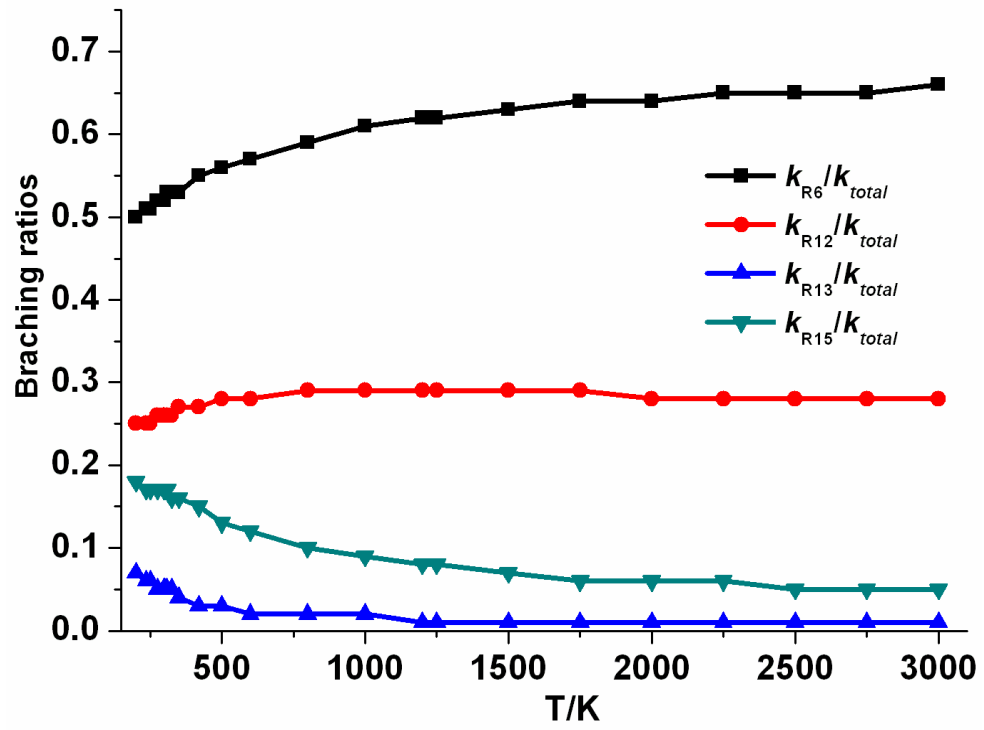
Fig. 8

Addition-elimination channels CH_3CHS+H_2O, CH_2CH_2+HSOH, $CH_3CHSO+H_2$ and CH_3CH_2SH+O are the major channels in the reaction between CH_3CH_2S and OH.